Clouds drive differences in future surface melt over the Antarctic ice shelves

Christoph Kittel [1], Charles Amory [2], Stefan Hofer [3], Cécile Agosta [4], Nicolas C. Jourdain [2], Ella Gilbert [5], Louis Le Toumelin [2,6], Hubert Gallée [2], and Xavier Fettweis [1]

[1]Department of Geography, UR SPHERES, University of Liège, Belgium
[2]Univ. Grenoble Alpes/CNRS/IRD/G-INP, IGE, Grenoble, France
[3]Department of Geosciences, University of Oslo, Oslo, Norway
[4]Laboratoire des Sciences du Climat et de l'Environnement, LSCE-IPSL, CEA-CNRS-UVSQ, Université Paris-Saclay, Gif-sur-Yvette, France
[5]Department of Meteorology, University of Reading, Whiteknights Rd, Reading RG6 6ET
[6]Univ. Grenoble Alpes, Université de Toulouse, Météo-France, CNRS, CNRM, Centre d'Études de la Neige, Grenoble, France

Correspondence: Christoph Kittel (ckittel@uliege.be)

S1 Shortwave and longwave radiation contributions

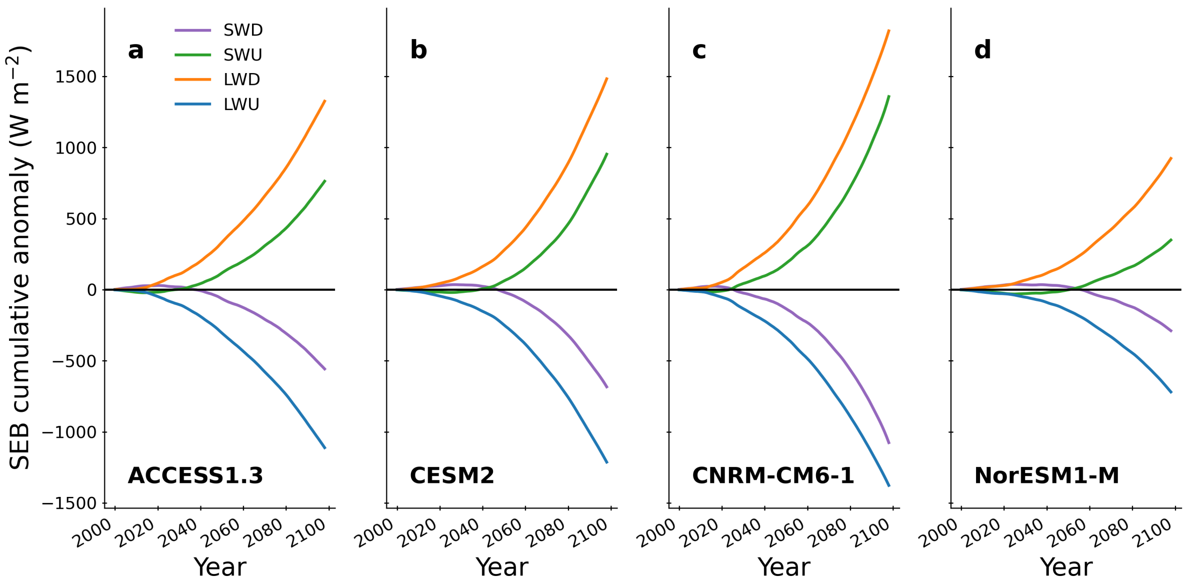

Figure S1. Cumulative summer melt and SEB radiation components converted into melt potential (Gt). Cumulative summer anomalies of melt, shortwave downwelling (SWD), shortwave net (SWN), longwave downwelling (LWD), and longwave upwelling (LWU) fluxes expressed as melt potential (Gt) projected by MAR driven by (a) ACCESS1.3, (b) NorESM1-M, (c) CNRM-CM6-1, (d) CESM2, compared to the reference 1981–2010 summer.

S2 Turbulent flux contributions

Both turbulent flux contributions firstly mitigate melt changes until 2070–2080 when latent heat exchanges tend to weakly increase melt only in MAR driven by CNRM-CM6 and CESM2 (Fig. 1). While the absolute SHF remains positive and then warms the surface in all our simulations during the 21st century, we find that SHF exchanges between the atmosphere and the surface are projected to weaken leading to a potential negative melt contribution. This has also been suggested by Donat-Magnin et al. (2021). A negative melt contribution for SHF is specific to the colder conditions in Antarctica as SHF should enhance melt over the Greenland ice sheet as a consequence of stronger barrier winds (Franco et al., 2013).

SHF varies according to vertical temperature gradient between the surface and the near-surface atmospheric layer, and wind that mixes this near-surface layer (Fig. S2). The summer mean near-surface wind speed over ice shelves is stationary in MAR driven by NorESM1, while it tends to decrease in the other experiments ($p<0.05$). The trends remain however weak compared to the present variability except when MAR is driven by CNRM-CM6-1. By absorbing radiative energy, the surface is projected to warm faster than the above near atmosphere reducing the temperature gradient until 2060. After 2060, our results suggest that wind speed could either still decrease in the relatively-colder projections (ACCESS1.3 and NorESM1-M) or increase in the warmer projections (CNRM-CM6-1, CESM2). SHF anomalies follow this pattern with decreasing potential melt contribution in all our experiments before diverging after 2060. We found a stronger association between SHF and the temperature gradient than with near-surface wind speed (see r values on Fig. S2). This suggests that the primary effect explaining SHF anomalies is the variation in the thermal inversion that can be modulated by wind shear changes. Furthermore, the more frequent presence of liquid water at the surface around the freezing point can reduce the temperature inversion or even warm the cold air advected by katabatic winds leading to negative SHF anomalies as already observed over the ice sheet (Kuipers Munneke et al., 2012; van Wessem et al., 2014).

The averaged values over all the Antarctic ice shelves however hide diverging local signals (Fig. S3). SHF are projected to decrease over most of the AIS, the peninsula excepted where SHF could significantly increase. Recent studies (Kuipers Munneke et al., 2012; van Wessem et al., 2014; Kuipers Munneke et al., 2018; Datta et al., 2019) have suggested that warm air advections (notably during foehn events) are an important source of energy over the Peninsula producing strong melt. Our results suggest an enhancement of the foehn effect due to warmer and moister air advections inducing higher precipitation (Kittel et al., 2021) but also larger melt rates. Since the snow/ice-covered surface cannot warm higher than the melting temperature, warmer air advections also increase the thermal inversion and then increase SHF. The positive SHF anomalies over the Peninsula become dominant for strong warmings projected to occur after 2060 when MAR is forced by CNRM-CM6 and CESM2 explaining the inversion of SHF anomalies in these two projections.

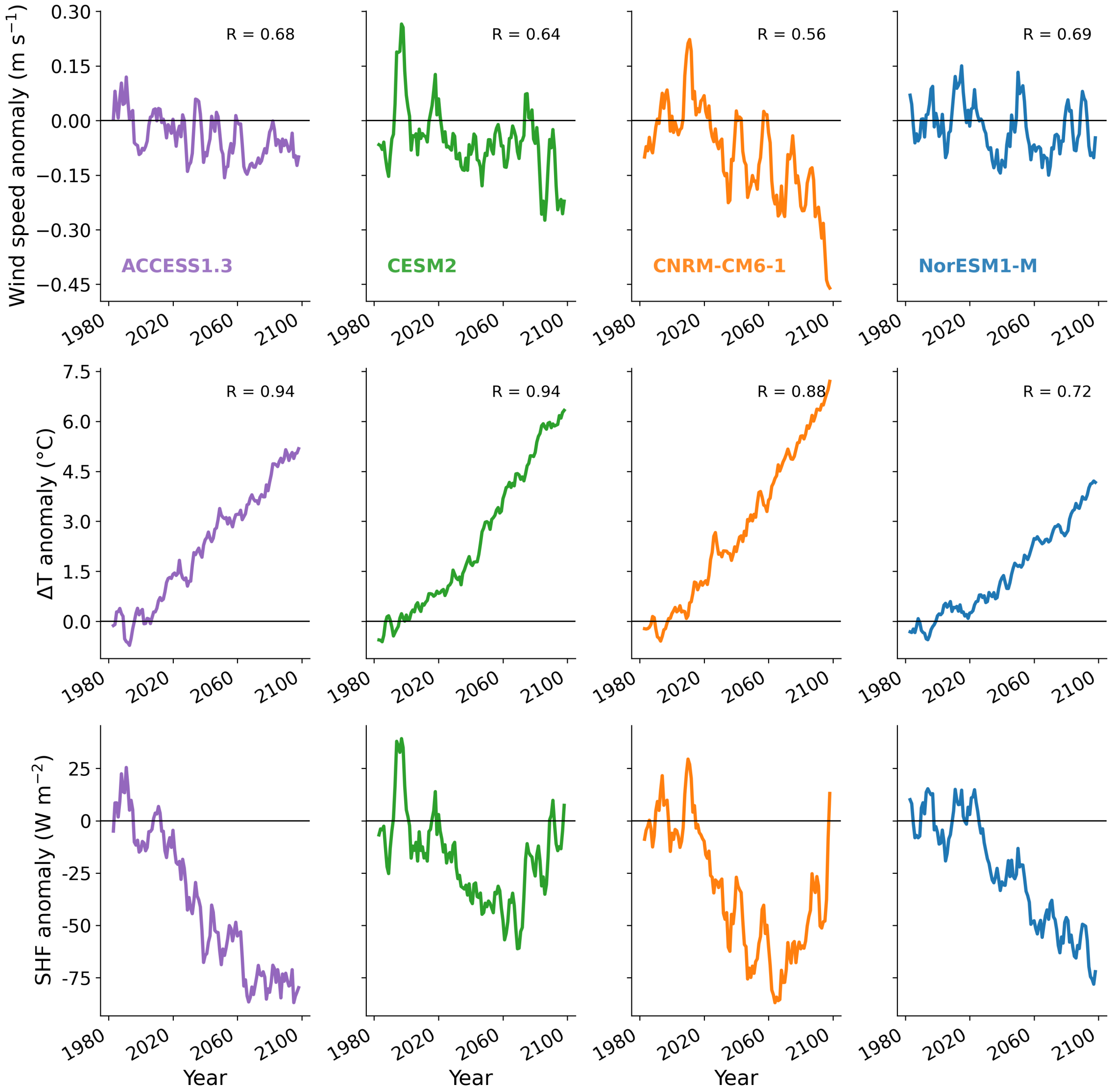

Figure S2. Summer changes in summer near-surface wind speed, temperature gradient and SHF over the ice shelves. Summer near-surface wind-speed anomalies ($\mathrm{m\,s^{-1}}$) (first row), temperature gradient between the first atmospheric level and the surface ($^{\circ}\mathrm{C}$) (second row), and sensible heat fluxes (expressed in melt potential $\mathrm{Gt\,3mo^{-1}}$) (third row) for MAR forced by ACCESS1.3 (purple), CESM2 (green), CNRM-CM6-1 (orange), and NorESM1-M (blue) compared to their summer mean value over 1981–2010. The correlation coefficients (R) between near-surface wind-speed and temperature gradient anomalies with SHF anomalies are also presented (p«0.01)

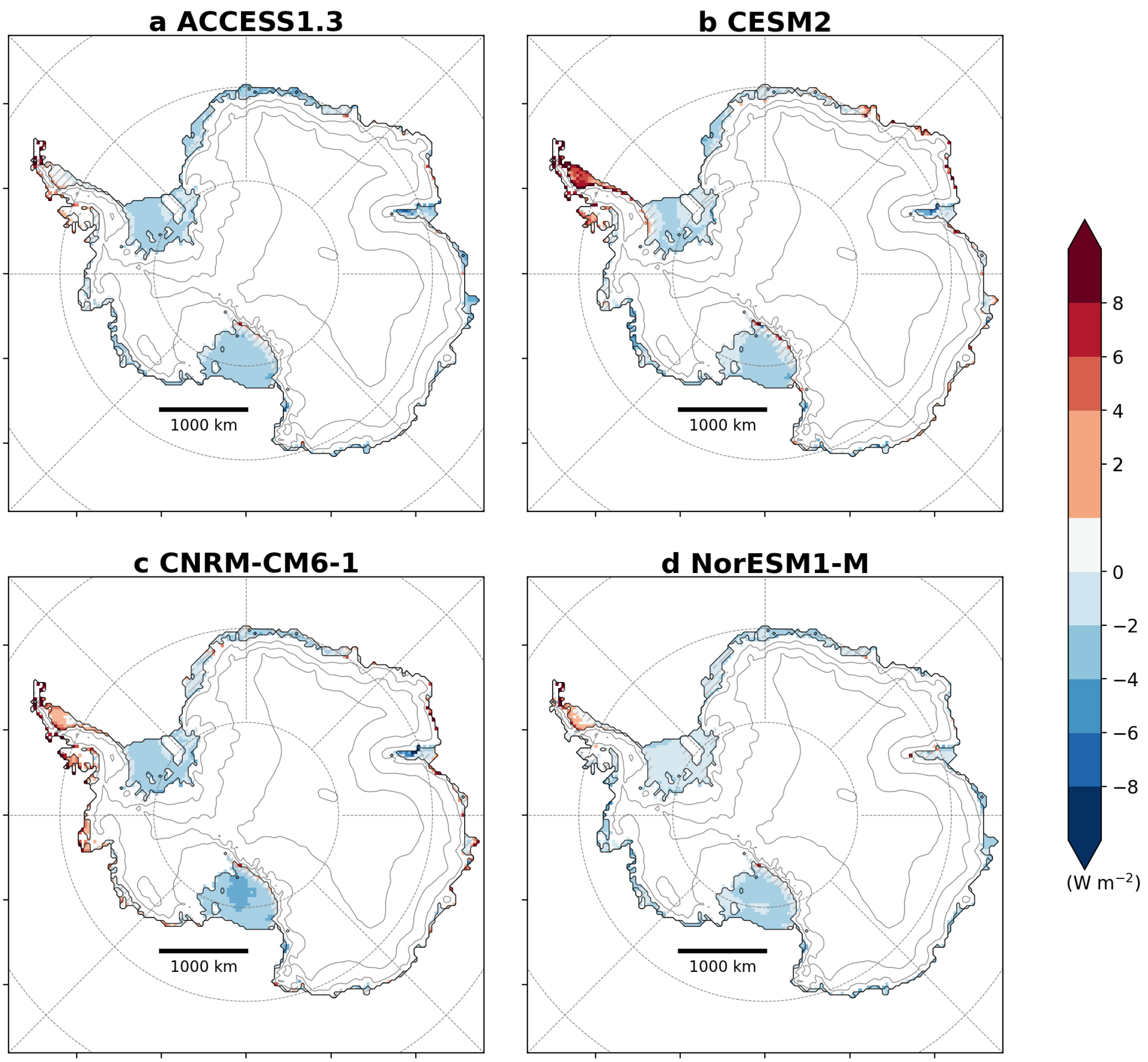

Figure S3. Summer changes in SHF. Summer SHF anomalies ($\mathrm{W\,m^{-2}}$) in 2071–2100 compared to 1981–2010 as projected by MAR driven by ACCESS1.3 (a), NorESM1-M(b), CNRM-CM6-1 (c), and CESM2 (d). Anomalies lower than the present variability (standard deviation) are hatched.

S3 Melt anomalies compared to near-surface temperature anomalies

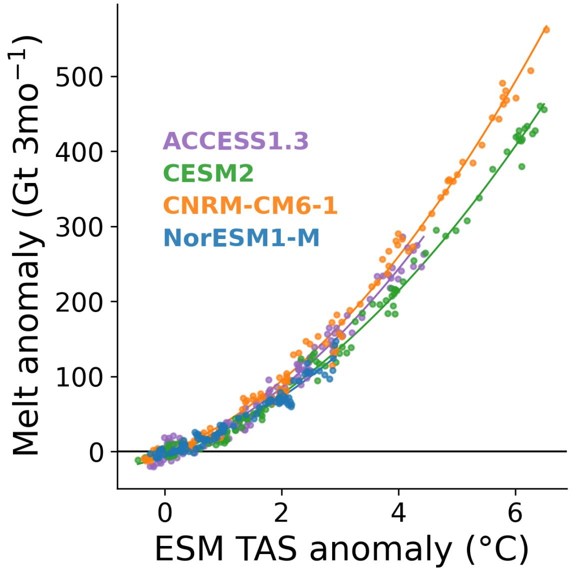

Figure S4. Association between summer melt anomalies ($\mathrm{Gt\,3mo^{-1}}$) projected by MAR over the Antarctic ice shelves and summer near-surface air temperature anomalies projected by the respective ESM forcing ACCESS1.3 (purple), CESM2 (green), CNRM-CM6-1 (orange), and NorESM1-M (blue)) between 90°S-60°S. The reference period is 1981–2010.

S4 Maximal contribution of summer atmospheric temperature

Approximating the atmosphere as a longwave-opaque and black body, we estimated the maximal potential contribution of the summer temperature of the atmosphere over the present (1981–2010) and the end of the 21st century (2071–2100) in Table S1. For instance, we found that the future atmospheric temperature in MAR forced by CESM2 and CNRM-CM6-1 could not explain more than 29% of modelled future LWD differences (1.5 $\mathrm{W\,m^{-2}}$ over to 5.1 $\mathrm{W\,m^{-2}}$).

Estimation of the maximal contribution of summer atmospheric temperature approximating the atmosphere as a longwave-opaque and black body (ε = 1) in equation 1:

$$LWDT = \varepsilon \times \sigma \times T^4, \tag{1}$$

Table S1. Near-surface summer mean temperature (TT) over the present and at the end of the 21st century, increased in LWD explained by the air temperature and simulated by MAR. Near-surface summer mean temperature over 1981–2010 ($^\circ\mathrm{C}$) (first column), over 2071–2100 ($^\circ\mathrm{C}$) (second column), increase in longwave downwelling radiation attributed to the increase in near-surface temperature ($\mathrm{W\,m^{-2}}$) (third column) and simulated (fourth column) by MAR driven by ACCESS1.3, CESM2, CNRM-CM6-1, NorESM1-M in 2071–2100 compared to 1981–2010.

ESM	$TT_{1981--2010}$ ($^\circ\mathrm{C}$)	$TT_{2071--2100}$ ($^\circ\mathrm{C}$)	$\Delta LWDT$ ($\mathrm{W\,m^{-2}}$)	ΔLWD ($\mathrm{W\,m^{-2}}$)
ACCESS1.3	-8.1	-4.0	+17.7	+23.2
CESM2	-8.1	-3.0	+22.4	+29.2
CNRM-CM6-1	-8.2	-2.7	+23.9	+34.3
NorESM1-M	-8.8	-5.8	+12.8	+17.3

S5 LWD anomalies compared to near-surface temperature anomalies

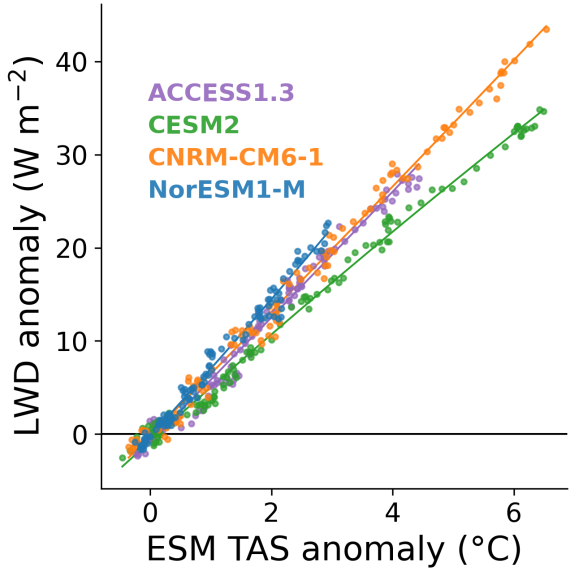

Figure S5. Association between summer LWD (W m^{-2}) projected by MAR over the Antarctic ice shelves and summer near-surface air temperature anomalies projected by the respective ESM forcing (ACCESS1.3 (purple), CESM2 (green), CNRM-CM6-1 (orange), and NorESM1-M (blue)) between 90°S-60°S. The reference period is 1981–2010.

S6 Water vapour path anomalies compared to near-surface temperature anomalies

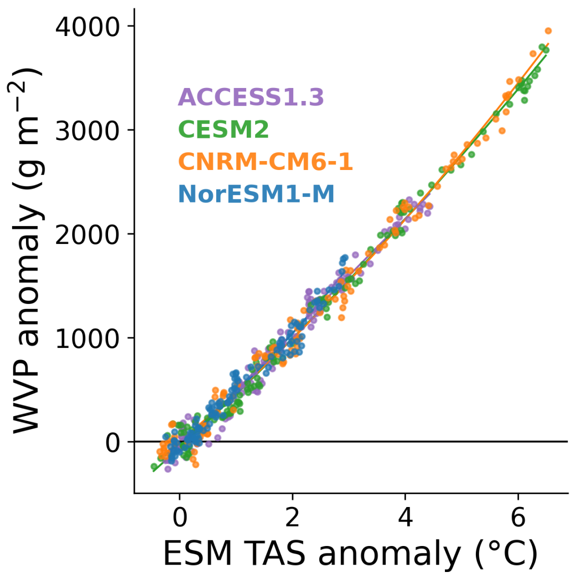

Figure S6. Association between summer Water Vapour Path ($\mathrm{g\,m^{-2}}$) projected by MAR over the Antarctic ice shelves and summer near-surface air temperature anomalies projected by the respective ESM forcing (ACCESS1.3 (purple), CESM2 (green), CNRM-CM6-1 (orange), and NorESM1-M (blue)) between 90°S-60°S. The reference period is 1981–2010.

S7 COD anomalies compared to near-surface temperature anomalies

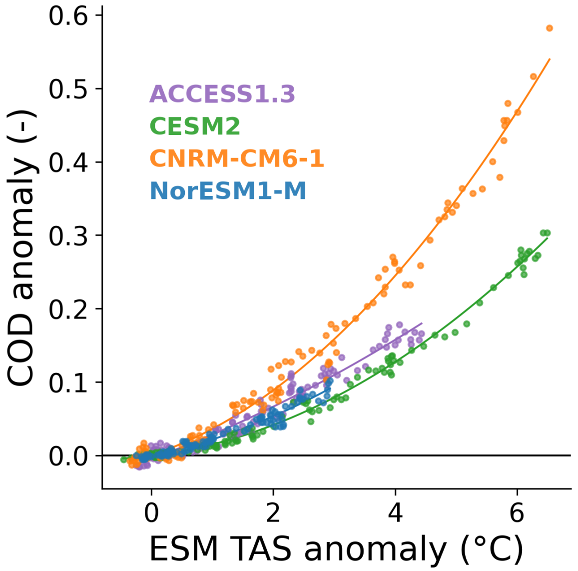

Figure S7. Association between summer cloud optical depth (-) projected by MAR over the Antarctic ice shelves and summer near-surface air temperature anomalies projected by the respective ESM forcing (ACCESS1.3 (purple), CESM2 (green), CNRM-CM6-1 (orange), and NorESM1-M (blue)) between 90°S-60°S. The reference period is 1981–2010.

S8 Future mean (vertical) changes in 2071–2100

Table S2. Mean changes in near-surface temperature, atmospheric specific humidity and temperature. Anomalies of summer near-surface air temperature ($^{\circ}\mathrm{C}$), atmospheric specific humidity ($\mathrm{g\,g^{-1}}$) and temperature ($^{\circ}\mathrm{C}$) between 925 hPa and 200 hPa in 2071-2100 compared to 1981-2010 as projected by MAR driven by ACCESS1.3, CESM2, CNRM-CM6-1, NorESM1-M.

ESM	$\Delta Near-Surface\,air\,Temperature$ ($^{\circ}\mathrm{C}$)	$\Delta Specific\,Humidity$ ($\mathrm{g\,kg^{-1}}$)	$\Delta Air\,Temperature$ ($^{\circ}\mathrm{C}$)
ACCESS1.3	+4.1	+0.30	+2.4
CESM2	+5.1	+0.47	+3.8
CNRM-CM6-1	+5.5	+0.44	+3.5
NorESM1-M	+3.0	+0.21	+1.7

References

Datta, R. T., Tedesco, M., Fettweis, X., Agosta, C., Lhermitte, S., Lenaerts, J. T., and Wever, N.: The effect of Foehn-induced surface melt on firn evolution over the northeast Antarctic peninsula, Geophysical Research Letters, 46, 3822–3831, 2019.

Donat-Magnin, M., Jourdain, N. C., Kittel, C., Agosta, C., Amory, C., Gallée, H., Krinner, G., and Chekki, M.: Future surface mass balance and surface melt in the Amundsen sector of the West Antarctic Ice Sheet, The Cryosphere, 15, 571–593, https://doi.org/10.5194/tc-15-571-2021, https://tc.copernicus.org/articles/15/571/2021/, 2021.

Franco, B., Fettweis, X., and Erpicum, M.: Future projections of the Greenland ice sheet energy balance driving the surface melt, The Cryosphere, 7, 1–18, 2013.

Kittel, C., Amory, C., Agosta, C., Jourdain, N. C., Hofer, S., Delhasse, A., Doutreloup, S., Huot, P.-V., Lang, C., Fichefet, T., and Fettweis, X.: Diverging future surface mass balance between the Antarctic ice shelves and grounded ice sheet, The Cryosphere, 15, 1215–1236, https://doi.org/10.5194/tc-15-1215-2021, 2021.

Kuipers Munneke, P., Van den Broeke, M., King, J., Gray, T., and Reijmer, C.: Near-surface climate and surface energy budget of Larsen C ice shelf, Antarctic Peninsula, The Cryosphere, 6, 353–363, 2012.

Kuipers Munneke, P., Luckman, A., Bevan, S., Smeets, C., Gilbert, E., Van den Broeke, M., Wang, W., Zender, C., Hubbard, B., Ashmore, D., Orr, A., King, J., and Kulessa, B.: Intense winter surface melt on an Antarctic ice shelf, Geophysical Research Letters, 45, 7615–7623, 2018.

van Wessem, J. M., Reijmer, C. H., Lenaerts, J. T. M., van de Berg, W. J., van den Broeke, M. R., and van Meijgaard, E.: Updated cloud physics in a regional atmospheric climate model improves the modelled surface energy balance of Antarctica, The Cryosphere, 8, 125–135, https://doi.org/10.5194/tc-8-125-2014, https://tc.copernicus.org/articles/8/125/2014/, 2014.